PAPER

Tailoring the electronic structure and magnetic properties of pyrochlore $Co_2Ti_{1-x}Ge_xO_4$: a GGA + *U ab initio* study

To cite this article: Sayandeep Ghosh *et al* 2021 *J. Phys.: Condens. Matter* **33** 145504

IOP Publishing Journal of Physics: Condensed Matter
J. Phys.: Condens. Matter **33** (2021) 145504 (12pp) https://doi.org/10.1088/1361-648X/abddfe

Tailoring the electronic structure and magnetic properties of pyrochlore $Co_2Ti_{1-x}Ge_xO_4$: a GGA + *U ab initio* study

Sayandeep Ghosh[1], Sobhit Singh[2], Debashish Das[1], Subhradip Ghosh[1], Pankaj Kumar Mishra[1] and Subhash Thota[1,*]

[1] Department of Physics, Indian Institute of Technology, Guwahati-781039, Assam, India
[2] Department of Physics & Astronomy, Rutgers University, Piscataway, New Jersey 08854, United States of America

E-mail: subhasht@iitg.ac.in

Received 19 November 2020, revised 4 January 2021
Accepted for publication 20 January 2021
Published 16 February 2021

Abstract

We report the electronic structure and magnetic properties of $Co_2Ti_{1-x}Ge_xO_4$ ($0 \leqslant x \leqslant 1$) spinel by means of the first-principle methods of density functional theory involving generalized gradient approximation along with the on-site Coulomb interaction (U_{eff}) in the exchange-correlation energy functional. Special emphasis has been given to explore the site occupancy of Ge atoms in the spinel lattice by introducing the cationic disorder parameter (y) which is done in such a way that one can tailor the pyrochlore geometry and determine the electronic/magnetic structure quantitatively. For all the compositions (x), the system exhibits weak tetragonal distortion ($c/a \neq 1$) due to the non-degenerate d_{z^2} and $d_{x^2-y^2}$ states (e_g orbitals) of the B-site Co. We observe large exchange splitting ($\Delta_{\text{EX}} \sim 9$ eV) between the up and down spin bands of t_{2g} and e_g states, respectively, of tetrahedral and octahedral Co^{2+} ($^4A_{2(g)}$(F)) and moderate crystal-field splitting ($\Delta_{\text{CF}} \sim 4$ eV) and the Jahn–Teller distortion ($\Delta_{\text{JT}} \sim 0.9$ eV). These features indicate the strong intra-atomic interaction which is also responsible for the alteration of energy band-gap (1.7 eV $\leqslant E_g \leqslant$ 3.3 eV). The exchange interaction ($J_{\text{BB}} \sim -4.8$ meV, for $(x, y) = (0.25, 0)$) between the Co^{2+} dominates the overall antiferromagnetic behaviour of the system for all 'x' as compared to J_{AA} (~ -2.2 meV, for $(x, y) = (0.25, 0)$) and J_{AB} (~ -1.8 meV, for $(x, y) = (0.25, 0)$). For all the compositions without any disorderness in the system, the net ferrimagnetic moment ($\Delta\mu$) remains constant, however, increases progressively with increasing x due to the imbalance of Co spins between the A- and B-sites.

Keywords: electronic structure, exchange interactions, spinels, antiferromagnetism

S Supplementary material for this article is available online

(Some figures may appear in colour only in the online journal)

1. Introduction

In the recent years, there is upsurge in the research on inverse spinel cobalt titanate (Co_2TiO_4) due to its unique catalytical activity and magnetic features such as negative magnetization, magnetic compensation, polarity reversal exchange-bias, re-entrant spin-glass behaviour etc [1–6]. Negative magnetization related to positive to negative sign change in dc-magnetization is generally observed in ferrimagnetic samples while cooling [7–9]. This phenomenon is observed due to different temperature dependence magnetization at different sites and at certain temperature the dc-magnetization becomes zero (negative to positive magnetization crossover) which is known as the compensation temperature (T_{Comp}).

* Author to whom any correspondence should be addressed.

Negative magnetization and the exchange bias have drawn the attention of the scientific community due to their potential applications in magnetic read/write heads, switching devices, magnetic random-access memory devices, spin-valves and various other spintronic devices [10–17]. Generally, the asymmetry in the magnetization versus magnetic field loops (also popularly known as exchange-bias field, H_{EB}) is a key feature noticeable in the compounds like $Co_2Ti(Sn, Ru)O_4$, $(NiCo)_{1-x}Zn_xFe_2O_4$, $CoFe_2O_4$ and $CoCr_2O_4$ and many more complex spinel oxides due to the couplings at the interface between the antiferromagnetic (AFM) phase and other magnetic phases such as ferromagnetic (FM), ferrimagnetic (FiM), or spin-glass (SG) [18–24]. In this paper we present *ab initio* calculations on the Ge substituted Co_2TiO_4 ($Co_2Ti_{1-x}Ge_xO_4$) and investigate the changes in electronic and magnetic properties as the structure is tuned from inverse FiM spinel (Co_2TiO_4) to normal pyrochlore AFM spinel ($GeCo_2O_4$).

Co_2TiO_4 crystallizes in an inverse-spinel structure belonging to space group Fd-$3m$, where the tetrahedral A-sites and half of the octahedral B-sites are occupied with the high spin state of Co^{2+} and Co^{3+} ion, respectively. Remaining half of the B-sites are occupied with the Ti^{3+} ion with $S = 1/2$ [5]. The temperature dependence of dc susceptibility ($\chi_{dc}(T)$) and heat capacity ($C_P(T)$) studies confirm a re-entrant SG behaviour ($T_{SG} \sim 46.8$) below the long range FiM ordering at $T \sim 48$ K along with a magnetic compensation phenomenon around $T_{Comp} \sim 32$ K [5, 6, 25–29].

In recent years there are surge in the interest of exploring the magnetic and electronic structure of Co_2TiO_4 due to improved experimental and computational techniques [30, 31]. Neutron diffraction studies reveal that the ground-state of Co_2TiO_4 exhibits a slight tetragonal distortion instead of the cubic symmetry due to the splitting of d_{xy} and d_{xz}/d_{yz} orbitals of the t_{2g} energy levels for both Ti^{3+} and Co^{3+} [6]. Fu *et al* experimentally investigated the influence of annealing temperature (T_A) on the crystal structure and magnetic properties of Co_2TiO_4 and demonstrated that the magnetic exchange interactions depend upon T_A and also reported a significant drop in T_{comp} as a result of the growth of tetrahedral sublattice due to high T_A [32]. Experimental studies involving the low temperature Arrott plot (H/M vs M^2) analysis from the M–H isotherms suggests pseudo first-order-transition, zero-crossover and the isothermal magnetic entropy change in Co_2TiO_4 below T_{comp} [25]. In addition, the $C_P(T)$ studies on this system reveal T^2 dependence at low temperatures ($\sim T < 15$ K) associated to the collective excitations of the spin-liquid state and very large geometrical frustration of the system [25].

On the other hand, end compound $GeCo_2O_4$ ($= (Ge^{4+})_A[2Co^{2+}]_BO_4$) has been widely investigated due to its unique magnetic properties such as, long-range AFM ordering below 22 K, Jahn–Teller distortion ($\sim$16 K), orbital frustration, and exclusive field-induced magnetic transitions [33–43]. The neutron diffraction studies indicate that due to the existence of the pyrochlore lattice of Co^{2+} ion, a complex structure of alternative planes of kagomé (KGM) and triangular (TRI) spins develop in the system [34–37]. The different types of exchange interaction in the KGM and TRI lattice planes generate the magnetic frustration in $GeCo_2O_4$ [34–37]. The temperature dependent magnetization and the specific heat analysis on this system reveal the presence of short-range 2D FM order near 100 K which is consistent with the specific heat studies performed by Lashley *et al* [41]. Using the high temperature magnetic susceptibility data, Pramanik *et al* calculated the magnitude of the dominant FM exchange constant ($J_1/k_B \sim 14.7$ K) [43]. The authors also determined the optical band-gap of the system which is nearly 3.2 eV using diffusive reflectance spectroscopy and supported the optical data with DFT calculations [43]. Interestingly, the field dependence analysis provides the evidence of magnetic field induced transitions at 11 kOe, 44 kOe and 97 kOe which is quite evident from the recent studies of Pramanik *et al* [43]. Besides the basic interesting physics, $GeCo_2O_4$ can be used as electrodes in the storage devices like Li-ion batteries which makes it an important compound to explore [43–45].

There are studies that suggest some interesting feature shown by Co_2TiO_4 when Ti is substituted with Ge [46–48]. For the compositions $x \geqslant 0.5$ generally polycrystalline samples ($Co_2Ti_{1-x}Ge_xO_4$) were unstable due to the presence of a small amount of $GeCo_2O_4$ [47, 48]. Strooper *et al* performed a detailed magnetization study on Ge substituted Co_2TiO_4 ($Co_2Ti_{1-x}Ge_xO_4$) and synthesized the fore-mentioned composition up to $x = 0.4$ [48]. These authors determined the first nearest neighbour exchange interaction between the A- and B-sites using both the paramagnetic susceptibility data and from the difference of two Brillouin functions on the spontaneous magnetization curves [48]. For the undoped case, they obtained the magnitudes of Curie constant as $C = 5.4601$ K cm^3 mol^{-1}, and exchange constants as $J_{AB} \sim -6.3$ K, $J_{AA} \sim -4.6$ K, and $J_{BB} \sim -5.5$ K. Motivated by these studies, in this work we present a detailed DFT based numerical investigations aiming to probe the electronic and magnetic structure of $Co_2Ti_{1-x}Ge_xO_4$ solid solutions. To the best of our knowledge such a theoretical study has not been reported in the literature to date. Our results fill the miscibility-gap ($0.4 \leqslant x \leqslant 1$) in the composition dependent phase diagram of $Co_2Ti_{1-x}Ge_xO_4$ which is essential to understand the electronic, crystallographic, magnetic structure of these solid solutions.

The organization of our paper is as follows. In section 2 we present the computational details. It is followed by the section 3: result and discussion where we present the numerical result related to our DFT calculation. Here we first present the crystal structure of Ge substituted Co_2TiO_4 which is followed by the electronic structure and magnetic properties of the investigated compound. Finally, we conclude in section 4.

2. Computational details

To probe the structural, electronic and magnetic properties of $Co_2Ti_{1-x}Ge_xO_4$ ($0 \leqslant x \leqslant 1$) we employed the density functional theory (DFT) studies as implemented in the Vienna *ab initio* Simulation Package (VASP) [49–53]. The crystal and electronic structure were optimized using the projector augmented wave (PAW) basis-set. We used the Perdew–Burke–Ernzerhof implementation of generalized gradient approximation (GGA) for exchange-correlation function

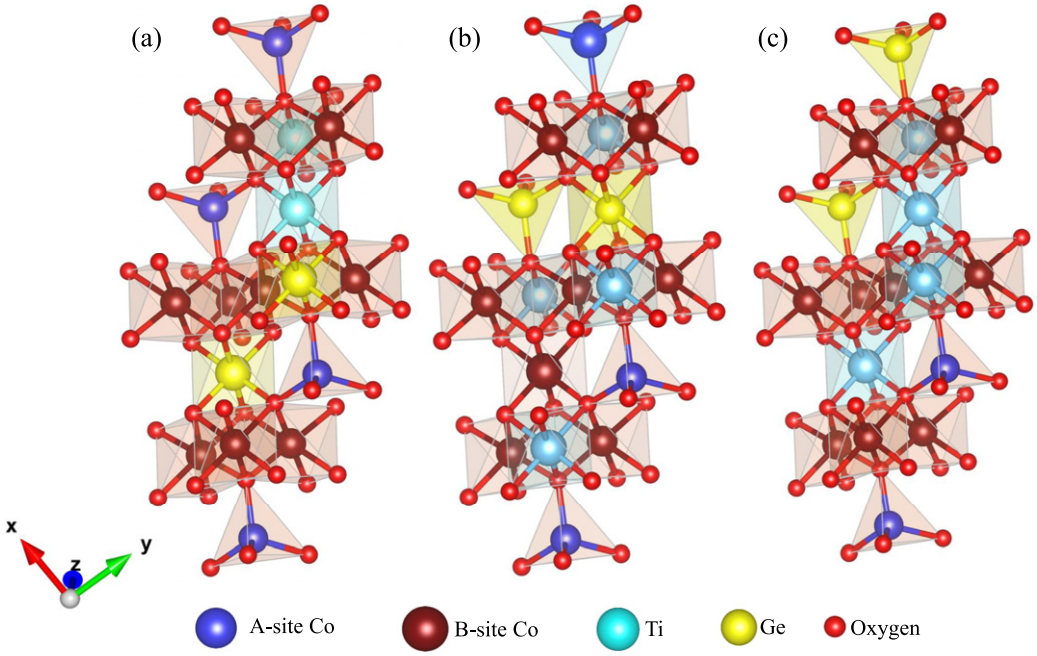

Figure 1. Schematic of the crystal structure of $Co_2Ti_{1-x}Ge_xO_4$ for different cationic disorder (a) $y = 0$, (b) $y = 0.5$, and (c) $y = 1.0$.

[54]. The valence electronic configurations used in PAW pseudopotentials were: Co ($3d^8 4s^1$), Ti ($3d^3 4s^1$), Ge ($4s^2 4p^2$), and O ($2s^2 2p^4$). The self-consistent calculations and the energy cut off 650 eV have been considered to perform the integration in the Brillouin zone. Due to the presence of strongly correlated d electrons we adopted the Dudarev's approach [55]. Accordingly, the effective Hubbard parameter is represented as $U_{\text{eff}} = U - J$, where U characterizes the on-site Coulomb correlation and J represents the Hund's coupling. In the present case all the calculations were performed by considering $U =$ 4 eV for both Co atoms, $U = 2$ eV for Ti atoms and $U = 0$ eV for Ge atoms [30], whereas, J is assumed to be 0 eV. The convergence criteria for the total energies and the forces on individual atoms were set to be 10^{-6} eV and 0.01 eV Å^{-1}, respectively.

As we are interested to probe the electronic and structural properties of Ge substituted Co_2TiO_4 system ($Co_2Ti_{1-x}Ge_xO_4$) for a wide range of compositions $x = 0$–1, a careful procedure is required to prepare the sample. Generally quasi-random methods [56, 57] and substitutional disorder techniques [58, 59] are used for such purposes. For our studies we have adopted the substitutional disorder technique for replacing the Ti with the Ge in the supercells. In brief we begin with a particular configuration of the parent compound and replace the Ti with Ge atoms at randomly chosen sites. Further we prepare several mental copies of the structure following the same procedure and compute the total energy of the system. We find that all the structures have same energy with negligible variation ($\sim 10^{-4}$eV) which indicate the formation of good samples. As we move from inverse spinel to normal spinel we introduce a parameter y which can be associated with measure of the cationic disorder. In the present study, we consider three different magnitudes of y namely (i) complete octahedral occupancy of Ge ($y = 0$), (ii) half-way occupancy of Ge atoms at both tetrahedral and octahedral sites ($y = 0.5$), and (iii) Ge atoms entirely occupying the tetrahedral sites ($y = 1.0$). To perform the simulations, initially we construct a supercell of Co_2TiO_4, which consists of 112 atoms ($16Co_A$, $16Co_B$, $16Ti_B$, and 64 O atoms) and for different value of x we substituted Ti with Ge atoms (see figure 1 and table 1S (https://stacks.iop.org/CM/33/145504/mmedia) [60]). In the present study, we considered different compositions of $Co_2Ti_{1-x}Ge_xO_4$ which can be expressed as: $(A_{1-xy}C_{xy})_{\text{tetra}}[B_{1-x}A_{1+xy}C_{x-xy}]_{\text{octa}}$.

In the following section we present our numerical results for electronic structure and magnetic properties of Ge substituted Co_2TiO_4.

3. Results and discussions

3.1. System free energy, equilibrium cationic disorderness and crystal structure

This section deals with the compositional and cationic disorder driven changes in the free energy of $Co_2Ti_{1-x}Ge_xO_4$ because it is very much necessary to determine the stable and energetically favourable ground state of the system for different compositions. Since both the end compounds Co_2TiO_4 ($x = 0$) and $GeCo_2O_4$ ($x = 1$) exhibit a slight tetragonal distortion at low temperatures [6, 42], it is worth to study the role of tetragonal distortion as well as degree of disorder on the physical properties of the pristine compound for different levels of Ge substitution. To find out the favourable structure we calculated the total energy as a function of c/a for eight different compositions and three different values of 'y'. Figures 2(a)–(d) show the total energy per formula unit (E/f.u.) as a function of c/a ratio. For $y = 0.0$, all the compositions show the lowest energy except for the $GeCo_2O_4$ system

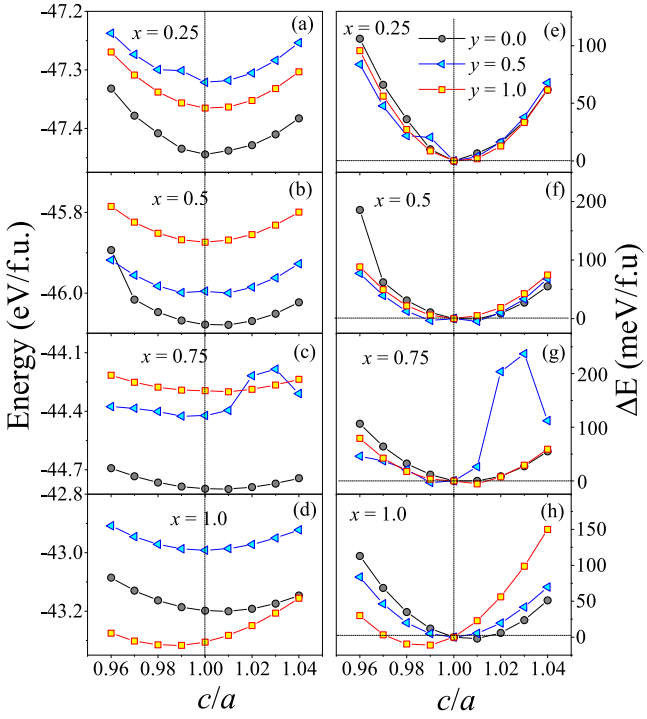

Figure 2. (a)–(d) Variation of total free energy (in f.u.) as a function of tetragonal distortion (c/a) ratio for different compositions of $Co_2Ti_{1-x}Ge_xO_4$. (e)–(h) Variation of ΔE ($=E(c/a=1) - E(c/a \neq 1)$) (meV/f.u.) as a function of tetragonal distortion (c/a) ratio for different compositions of $Co_2Ti_{1-x}Ge_xO_4$.

($x = 1.0$) which exhibits the lowest energy for $y = 1.0$ and is in-line with the recent experimental observations [43]. It is quite interesting to see that for all the compositions, Ge are favourable to occupy the octahedral B-sites, but at the vicinity of the phase boundary ($x = 1.0$) they prefer the tetrahedral A-sites. As the structure changes from inverse to normal spinel the E/f.u. gradually decreases independent of any y value for $x = 0.125$ ($y = 0$) the value of E/f.u. $= -48.10$ eV and for $x = 0.875$ ($y = 0$) the value of E/f.u. $= -44.15$ eV. The corresponding energy difference between the two configurations is $\sim$0.11 eV ($e = (\text{E/f.u.})_{y=1} - (\text{E/f.u.})_{y=0}$) considering no tetragonal distortion ($c/a = 1$). This energy difference e, gradually increases and attains maximum of $e =$ 0.5 eV and 1.48 eV for $x = 0.75$ and $x = 0.875$, respectively. Such changes become quite significant as system composition approaches close to the pyrochlore stable region of $GeCo_2O_4$ in which competing exchange interactions play a significant role which as a result for $y = 1.0$ shows higher energy with respect to the other values of y. The experimental results based on temperature dependence of specific heat measurements on similar type of systems reported that the low-temperature disorder in the ground state is essentially induced by magnetic frustration [41, 61].

To probe the tetragonal distortion present in the system we calculated the energy difference between the cubic structure ($c/a = 1$) and tetragonally distorted unit cell ($c/a \neq 1$) ($\Delta E = E(c/a = 1) - E(c/a \neq 1)$) and plotted it as a function of c/a ratio, as shown in figures 2(e)–(h). Here the pristine compound ($x = 0$) with only one configuration, that is Ti^{4+} ions at octahedral B-sites exhibit the lowest energy configuration under tetragonal configuration than the cubic structure (with $c/a > 1$) which is in-line with the recent neutron diffraction studies reported on the single crystals of Co_2TiO_4 [6]. For $y = 0.0$ (complete B-site disorder), for dilute dispersion of Ge ($x = 0.125$) in the spinel lattice, the system crystallizes in perfect cubic structure without any tetragonal distortion. However, with increasing Ge content the system exhibits slight distortion. As for an example, for $y = 0.5$ (partial B-site disorder situation), the system energetically favours cubic structure up to some moderate compositions $x \leqslant 0.25$. Nevertheless, the system remains tetragonal distorted with $c/a > 1$ up till $x = 0.75$, but beyond $x = 0.75$ system exhibits $c/a = 0.99$, slight shrinkage in the tetragonal unit cell due to the different ionic radius of the cations Ge and Ti. For $y = 1.0$ (complete A-site disorder), depending upon the composition the overall system oscillates its energetically favourable situation between the tetragonal and cubic structure. For example, the combination of $y = 1.0$ and $x = 1.0$ causes the system to stable with $c/a < 1.0$, which is in contrast with the earlier experimental observations where the authors noticed a giant tetragonal distortion with $c/a \sim 1.4$ [42]. As a special case our calculations with the experimental lattice parameters yield very high magnitude of E/f.u. signifying the fact that the experimentally obtained parameters are not effective at low-temperatures especially at absolute temperature where the calculated results are valid. Regardless of any composition of y and x values the c/a of this interesting spinel system oscillates between 0.99 and 1.01 signifying mild tetragonal distortion persists in the system (see figure 2(h)). For $x = 1$, that is pyrochlore $GeCo_2O_4$ case where Ge atoms disperses from $y = 0.0$ (B-site) to $y = 1.0$ (A-site), we noticed a systematic change in c/a ratio. In the following we discuss this scenario more clearly in terms of partial density of states (DOS) of octahedrally coordinated Co ions.

In order to confirm the most stable ground state configuration we calculated the formation energy of the system for three different values of $y = 0.0, 0.5$ and 1.0 (see the inset of figure 3(a)). Generally, the ground state formation energy was determined from the energy difference between the alloy and the sum of the total energies of elements in its actual solid form of weighted over concentration using the formula:

$$E_{\text{form}} = E_{Co_2Ti_{1-x}Ge_xO_4} - 2E_{\text{Co}} - (1-x)E_{\text{Ti}} - xE_{\text{Ge}} - 4E_{Oxy}. \quad (1)$$

Here, the first term is the total energy in formula unit of the supercell, whereas the last four terms are the individual energies corresponding to the elements Co, Ti, Ge and O atoms, respectively. These results are in good agreement with previous analysis discussed above pertaining to the energy minimization calculation. For $x = 0.125$ with perfect inversion the formation energy exhibits minimum value of the order of -22.67 eV and the formation energy gradually decreases to -19.42 eV with increasing the Ge substitution for all the values of y. For $x = 1.0$ without any inversion ($y = 1.0$) the system possesses lowest energy of ~ -18.75 eV. In order to examine the site occupancy of Ge atoms in $Co_2Ti_{1-x}Ge_xO_4$ system, we propose two distinct ways. The first possibility

is 'Ge' atoms occupy the tetrahedral site only for $x = 1$ and second possibility is that they start occupying the tetrahedral sites over a range of compositions before it attains perfect pyrochlore structure, such small zone of compositions (δx) is referred to as morphotropic phase boundary.

Generally, the degree of cationic disorder 'y' at any finite temperature can be calculated from the thermodynamic consideration of cation distributions by treating it as a simple chemical equilibrium configuration [62]. Following Navrotsky and Kleppa, we have used the configurational free energy of cation disorder per formula unit (ΔF) as $\Delta F = E_c - T\Delta S_c$, where the E_c is cation disorder energy per formula unit, T is the sintering temperature, $\Delta S_c = -k_B \sum_{i,b} p_i^b \ln p_i^b$ is the configurational entropy, and p_i^b is the concentration of the cations b at the i^{th} sub-lattice [62]. In the present case the cation disorder energy, E_c, represents the energy difference between the inverted state and the other disorder states. In order to get the dependence of E_c on y we fitted E_c with a quadratic relation $E_c = \alpha y + \beta y^2$, where α and β are the constants. Following the Kriessmen and Harrison method of quadratic dependence of the cation disorder energy we determined the E_c for $y = 0, 0.5$ and 1 for different values of x [63]. As a second step these energies are fitted with the quadratic relation mentioned above which yield the variation of E_c for entire range of y. At the equilibrium the degree of cation disorder parameter (y_0) for any temperature is obtained by minimizing the configurational free energy, ΔF, with respect to y. Using this formalism further we have evaluated y_0 for different compositions. Figures 3(a) and (b) show the variation of E_c and ΔF with y for different Ge concentration x at sintering temperature $T = 1250$ K [48]. The variation of E_c as a function of y shows nearly identical trend for all the x values below 0.75. However, for higher compositions close to the morphotropic phase boundary $E_c(y)$ displays parabolic variation, specifically for $x = 0.875$ such trend is more prominent, as the difference between the cation disorder energy is significantly high ($E_c \geqslant 1.8$ eV/f.u). This particular feature indicates that the disorderness play an important role in the formation energy. In the present case E_c varies between 0 and 0.4 eV/f.u for lower compositions, whereas, E_c reaches more than 1.8 eV/f.u for higher compositions. For all the cases except $x = 1.0$, E_c attains minimum at $y = 0.0$ which is quite consistent with our previous analysis. Similarly, the $\Delta S_c(y)$ plot (see figure 1S) [60] reveal gradual increase of entropy with y and for most of the compositions the maximum value of change in entropy lies between $y = 0.5$ and 0.8. However, by considering the configurational entropy of the system, we obtained slightly different result in case of $\Delta F(y)$ (figure 3(b)) as compared to $E_c(y)$. Summing-up all this variation, in the inset of figure 3(b) we show the compositional dependence of equilibrium cation disorder ($y_0(x)$) which infers that the Ge atoms are more favourable to B-site occupancy rather than A-site for low ($x < 0.3$) and intermediate compositions ($0.3 \leqslant x \leqslant 0.75$) with an anomaly between $x = 0.45$ and 0.55, whereas for $x > 0.875$, Ge atoms start occupying the A-sites. Nonetheless, a sharp increase in the y_0 is clear as x approaches the morphotropic phase boundary shown by the yellow highlighted region before reaching

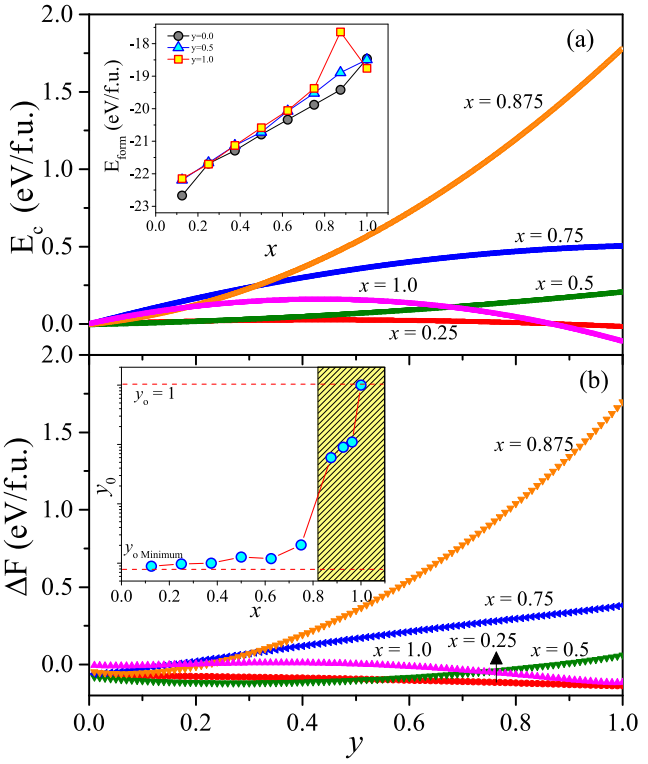

Figure 3. Variations of (a) cation disorder energy (E_c) and (b) configurational free energy (ΔF) with respect to the cation disorder parameter (y) of $Co_2Ti_{1-x}Ge_xO_4$, for different compositions 'x' at $T \sim 1250$ K, the sintering temperature of the sample. Inset of figure (a) and (b) shows the calculated formation energy (E_{form}) and the variations of the equilibrium cationic disorder (y_0) for different compositions of $Co_2Ti_{1-x}Ge_xO_4$, respectively.

the final stable pyrochlore structure with 100% Ge atoms at tetrahedral A-sites.

After determining the ground state configuration of the system $Co_2Ti_{1-x}Ge_xO_4$, we turn our focus on the crystal structure, bond-lengths and the variation of lattice parameter as a function of x and y. In table 2S we list the lattice parameters a, c and cation–anion bond lengths for different values of x and y [60]. Accordingly, the lattice parameters a (and c) obtained from DFT + U calculations are 8.54 Å (8.62 Å) and 8.50 Å (8.42 Å) for $x = 0$ and 1, respectively. These values are slightly higher than those reported earlier using x-ray diffraction measurements which could be due to the choice of GGA while considering the exchange correlation part in the Hamiltonian [5, 30, 43]. For $y = 0$, we obtained $a \sim 8.54$ Å for $x = 0.0$ which decreases to 8.48 Å for $x = 1.0$ due to the smaller in the ionic radius of Ge^{4+} (~0.53 Å) as compared to Ti^{4+} (~0.61 Å). However, for the case of $y = 0.5$ and 1, a non-linear trend was observed in which lattice parameter 'a' varies between 8.4 Å and 8.6 Å due to unstable structure driven by the cation disorder. But under the limit of dilute dispersion ($x \leqslant 0.125$) of Ge, system retains almost cubic structure for all the values of y without any distortion, and exhibits departure from cubic structure as the Ge substitution increases in Co_2TiO_4 with slight tetragonality. Interestingly, for certain combinations of x and y we observed that the lattice parameter c is much smaller than the a. Ascribed to the lower co-ordination

number of A-site Ge^{4+} and shrinkage of ionic radius to 0.39 Å as a consequence one may notice minor changes in the lattice parameters a and c (table 2S) [60]. For the case of $x = 1.0$, the contraction of $[Co]_{oct-O}$ bond length is significant along the z-axis hence one may expect decrease of 'c', however, the $[Co]_{oct-O}$ bond length expands in the xy-plane giving rise to unequal lattice constants leading to c/a ratio deviating from unity.

For $x = 0$ (Co_2TiO_4) we obtained the bond-lengths $[Co]_{A-O}$ (1.99 Å) are less than $[Co]_{B-O}$ (2.11 Å) which are in line with the previously reported data [5, 30]. These results are quite obvious as the effective ionic radius of high-spin Co^{2+} state is 0.58 Å and 0.75 Å at A and B-sites, respectively. However, the bond lengths do not change significantly with the variation of x and y. For the $[Co]_{A-O}$ case the average bond length varies between 1.96 Å and 2.00 Å, whereas, for the octahedral site the average bond length between Co and O varies between 2.10 Å and 2.12 Å associated with the weak Jahn–Teller like distortion. The low spin Ge at the tetrahedral A and octahedral B-sites (with tetravalent electronic state) exhibits large difference in the effective ionic radius of 0.39 Å and 0.53 Å, respectively. As a result, the average bond length of $[Ge]_{A-O}$ (∼1.83 Å) is significantly lower than $[Ge]_{B-O}$ (∼1.97 Å). Therefore, the average bond lengths of the cation and anions at octahedral sites display systematic decreasing trend ($[Co]_{B-O} > [Ti]_{B-O} > [Ge]_{B-O}$) with the Shannon ionic radius of the atoms ($R_{Co^{2+}} \sim 0.75$ Å $> R_{Ti^{4+}} \sim 0.61$ Å $> R_{Ge^{4+}} \sim 0.53$ Å).

To understand the origin of slight tetragonal distortion present in the $Co_2Ti_{1-x}Ge_xO_4$ system we interpret the data based on the crystal field theory reported by Dunitz and Orgel [64]. Accordingly, the tetragonal distortion and cubic symmetry mainly depend on the electronic configurations of the cations occupying the tetrahedral and octahedral sites. In the present case, the A-site Co^{2+} have the electronic configuration $(e_g)^4(t_{2g})^3$ while B-site Co^{2+} configuration is $(t_{2g})^5(e_g)^2$. Since, the Ge^{4+} and Ti^{4+} do not have any d electron so their atoms do not contribute in the tetragonal distortion. From the crystal field theory, it is quite clear that the weak tetragonal distortion is plausible due to the presence of Co^{2+} atom in B-site, whereas, the Co^{2+} atom in A-site do not have any contribution. Now, as we increase the cation disorder y, the presence of tetragonal distortion increases progressively due to the increasing occupancy of Co atoms at the B sites. As a result, the degeneracies associated with the e_g orbitals increases significantly ($c/a \neq 1$), indicating the presence of tetragonal distortion for all the compositions with $y = 0.5$ and 1 (figure 2).

In the following section, we will utilize this information related to the distance between cation and anion to understand the crystal field parameter (Δ) more precisely.

3.2. Electronic structure and magnetic behaviour: disorder and composition driven changes

In this section we discuss about the variation of electronic density of states (DOS) and magnetic properties by focussing the compositional variation and the dependency of cation disorder. Figure 4 show the DOS of $Co_2Ti_{1-x}Ge_xO_4$ for stable ground state configurations for x and y. The DOS corresponding to Co and Ti play a significant role as compared to the Ge states which is quite negligible. For pure Co_2TiO_4 ($x = 0$), the top of the valence band mainly consists of t_{2g} majority band of the octahedral Co. The majority and minority spin configurations of t_{2g} and e_g of tetrahedral and octahedral Co, respectively lie deep inside the valence band (∼6 eV). Due to this reason, a large exchange splitting ($\Delta_{EX} \sim 8$ eV) has been observed for the Co atoms occupying at both A and B sites. In addition, the feature of DOS plots confirm the t_{2g} states of A-site Co are half filled and the e_g states are completely filled. Whereas, in case of B-site Co ions, the e_g states are half filled and t_{2g} states are more than half filled which left with only one unpaired electron. On the other hand, the conduction band maxima (∼1.5 eV) dominated by the up and down spin of t_{2g} states of Ti along with the A-site Co states. It is interesting to note that the hybridization between the O-2p and Co-3d orbitals is evident across the valence band (at ∼−2.5 eV). In general, for any combination of x and y of the investigated system, the splitting in t_{2g} and e_g symmetries due to the crystal field is clearly noticeable in the DOS versus energy plots (figure 4). Although the contribution of Ge DOS is minimal but its incorporation in the Co_2TiO_4 matrix makes noticeable change in the shift of the orbital energies which further creates non-degenerate states responsible for the degree of tetragonality in the system. For all x, Co exhibit high spin ($S = 3/2$) configuration with divalent oxidation state for both tetrahedral A and octahedral B sites, therefore the behaviour of DOS is nearly similar except for few compositions noticeable shift in both t_{2g} and e_g states is palpable. For $y = 0$, $x = 0.125$ the splitting of majority t_{2g} states of B-site Co is very clear and for higher compositions the splitting in the t_{2g} band is much prominent. Also, the splitting in minority spin e_g states of B-site Co (∼6 eV, due to non-degenerate d orbitals) is observed for all the combination of x and y. Close examination of the DOS reveals that the $d_{x^2-y^2}$ and d_{z^2} orbitals of e_g states in B-site Co have become non-degenerate while $d_{x^2-y^2}$ exhibits lower energy than the d_{z^2} orbitals implying the presence of tetragonal distortion of the system with c/a ratio greater than 1. For $y = 0$, for all the values of x we observed non-degenerate orbitals in e_g states, although, the splitting in t_{2g} is most significantly visible for $x > 0.25$ only. Similar behaviour is observed in case of the t_{2g} states of Ti atoms in the conduction band (∼1 eV). For low compositions, the sub-bands are suppressed but with increasing the Ge substitution ($x \geqslant 0.75$) the electronic states gradually populate-up and the splitting is substantial (see figure 4). This feature clearly suggests that Ti ions equally contribute to the tetragonal distortion along with the octahedral Co and they also play an important role in deciding the crystal structure. In the following we discuss the tetragonal distortion of the system in a detailed manner.

For $y = 0.5$, the overall DOS of the system exhibits delocalization behaviour of different wave functions which is evident from the figure 2S as compared to the disorder less situation ($y = 0$) which has clearly distinguishable total DOS. Similar features have been observed in case of atom projected DOS of Co ions located at tetrahedral A-sites and octahedral B-sites. However, the majority t_{2g} states of A-site Co ions

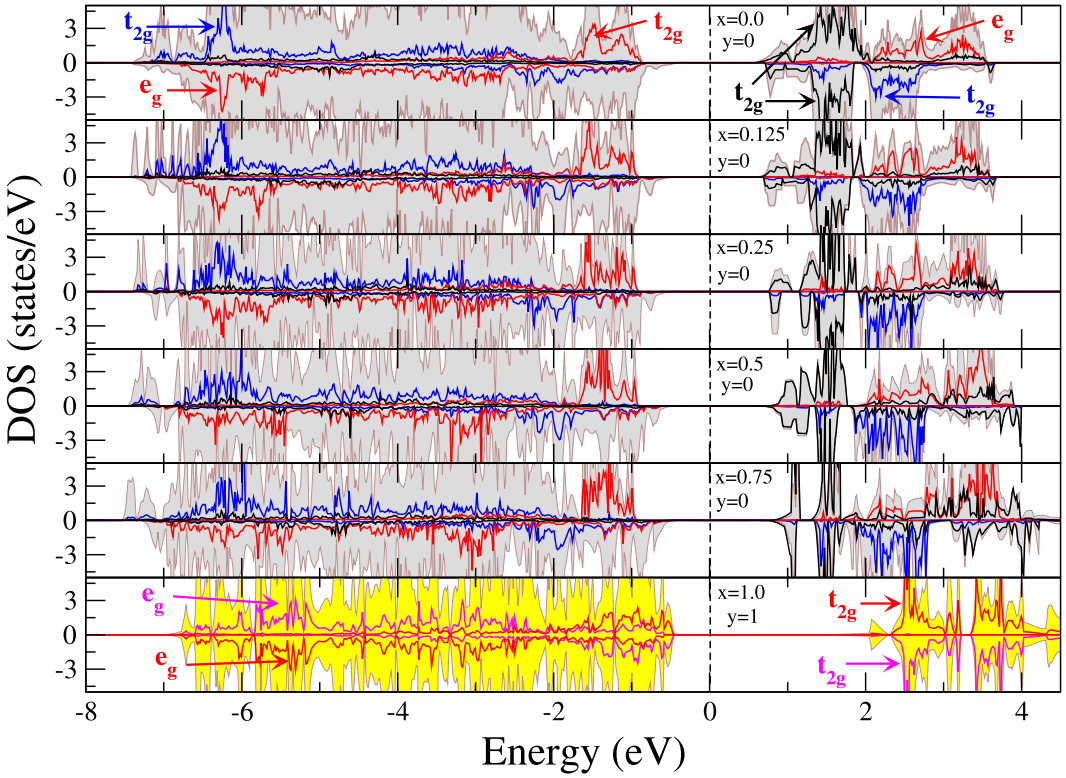

Figure 4. Calculated DOS for stable ground state configurations of x and y. The total DOS is represented using the brown line. The blue and red lines represent the DOS of Co present in A- and B-site, respectively. The solid black colour plots represent the B-site Ti. For $x = 1.0$ the solid magenta line represents the contribution from other octahedral Co. Dotted vertical lines at $E = 0$ depicts the Fermi level (E_F). The partial DOS of Ge is not visible due to low intensity.

shifted towards the lower energy side with the incorporation of Ge: for $y = 0.5$, $E \sim -6$ eV and -5.5 eV for $x = 0.125$ and 0.75, respectively. Similarly, a small shift in energy levels for majority t_{2g} states of B-site Co ions is observed across -1 eV. Nevertheless, in the case of Ti atoms an interesting feature of the DOS is observed for $x = 0.25$ and 0.75; that is the electronic states of Ti atoms are dominated at the top of the valence band (∼0.8 eV) and the splitting of $d(t_{2g})$ orbitals is quite clearly visible. However, for $x = 0.50$, the Ti states are situated deep into the conduction band (∼1.5 eV from E_F). Similar behaviour has been observed in case of completely disordered system (i.e. all the Ge atoms are in tetrahedral sites $y = 1.0$) for different compositions except for complete substitution of Ge atoms at Ti. Moreover, for $x = 1.0$, the up-spin and down-spin states of the Co atoms are symmetric to each other indicating perfect AFM (↑↓) arrangement of spins which is consistent with the previously reported experimental observations [30]. All the compositions for $y = 0.5$ and $y = 1.0$ (except $x = 1.0$), the DOS clearly reveal the delocalization of the different atomic wave functions which indicate the instability of the compositions (figures 2S and 3S). Due to this reason the entropy of the systems shows higher value with respect to $y = 0$ case. Consequently, the calculated configurational free energy is relatively high. Therefore, we can conclude that experimentally the formation of the solid solutions with disorder parameters $y = 0.5$ and $y = 1.0$ is not possible and these remarks are in-line with the formation energy calculations as discussed.

Figure 5 shows the DOS associated with the d_{z^2} and $d_{x^2-y^2}$ of e_g orbitals of octahedral Co for $x = 1$ for different cationic disorder. It is important to depict this figure because the octahedral Co ions are the main source of tetragonal distortion present in the system due to its electronic configuration ($(t_{2g})^5(e_g)^2$). For $y = 0$, the down spin of d_{z^2} orbitals in the valence band exhibits lower energy with respect to the down spin state of $d_{x^2-y^2}$ orbitals resulting $c/a > 1$. For $y = 0.5$ case, it is hard to differentiate between the degenerate states of d_{z^2} and $d_{x^2-y^2}$. As a result, the system stabilizes in the cubic structure, however, the system exhibits weak tetragonal distortion for $y = 1.0$. But, in this case the $c/a < 1$ as the energy level corresponding to the non-degenerate d-states with higher energy of d_{z^2} than that of $d_{x^2-y^2}$. Thus, switching of c/a ratio between less than one and/or greater than one suggests the crucial role of Ge atom in deciding the tetragonal distortion of the investigated system (for $0 \leqslant y \leqslant 1$). Similarly, the splitting of d_{z^2} and $d_{x^2-y^2}$ orbitals controls the c/a ratio for different compositions $0 \leqslant x \leqslant 1$ for specific y.

Figure 6 shows the exchange splitting (Δ_{EX}) and crystal field splitting (Δ_{CF}) parameters for the energetically favourable compositions of $Co_2Ti_{1-x}Ge_xO_4$ system. We evaluated both the parameters Δ_{EX} and Δ_{CF} from the DOS calculations using: (i) $\Delta_{EX}^{e_g} = e_g^{\uparrow} - e_g^{\downarrow}$, (ii) $\Delta_{EX}^{t_{2g}} = t_{2g}^{\uparrow} - t_{2g}^{\downarrow}$, (iii) $\Delta_{CF}^{\uparrow} = e_g^{\uparrow} - t_{2g}^{\uparrow}$, and (iv) $\Delta_{CF}^{\downarrow} = e_g^{\downarrow} - t_{2g}^{\downarrow}$ [30, 65–67]. In case of A-site Co the exchange splitting linked to the t_{2g} states are much stronger than the e_g states and the

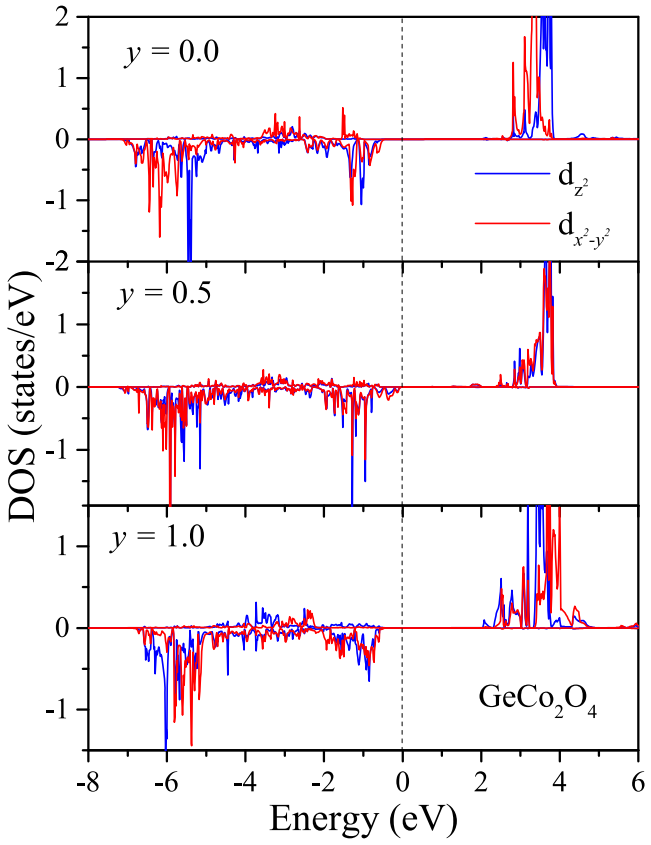

Figure 5. Calculated DOS versus energy (E) plots for octahedral Co in $GeCo_2O_4$ system for different values of y.

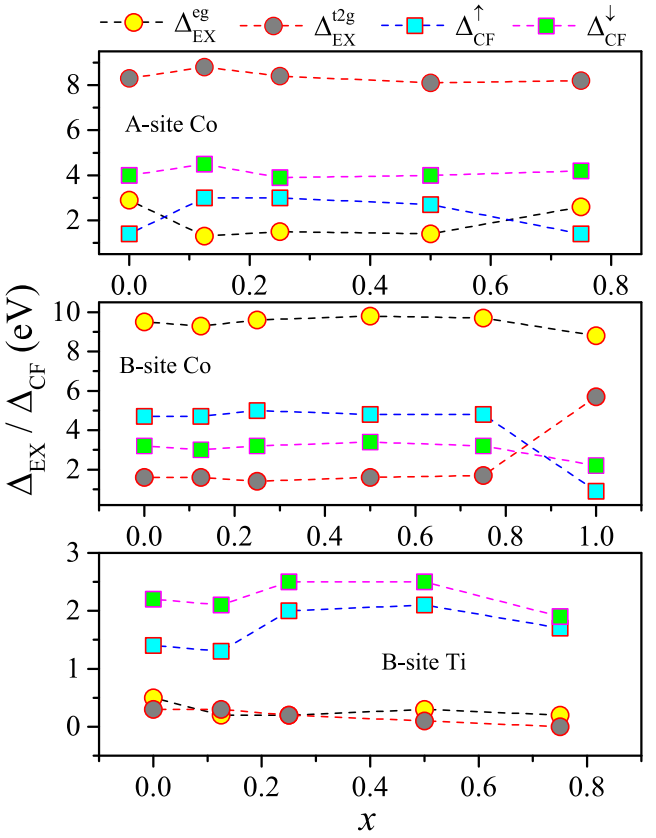

Figure 6. The calculated exchange splitting (Δ_{EX}) and crystal field splitting (Δ_{CF}) for different compositions (x) of $Co_2Ti_{1-x}Ge_xO_4$.

low crystal field splitting (∼4 eV) causes the high spin state of Co. On the contrary, for the octahedral Co we noticed the opposite feature ($\Delta_{EX}^{e_g} > \Delta_{EX}^{t_{2g}}$). Nonetheless, the magnitude of Δ_{EX} and Δ_{CF} almost remains same due to the localization of the d orbitals. In case of the octahedral Co, the crystal field splitting decreases for $x = 1.0$ and this occurs due to the increase of bond-length of Co_{oct}–O. It is well known that the crystal field of the octahedral site is inversely proportional to the distance between the cation and anion ($\Delta \sim 1/(B-O)^5$). For the octahedral Ti, Δ_{EX} is nearly negligible as the up spin and down spin of t_{2g} and e_g states are degenerate, as a consequence the centres of this state lie approximately at the same energy level, hence the Δ_{CF} is always greater than Δ_{EX}. Importantly, this analysis leads to the inference that different magnitude of exchange splitting and crystal-field splitting in $Co_2Ti_{1-x}Ge_xO_4$ system does not have any significant change in the profile of $\Delta_{EX}^{e_g}(x)$ and $\Delta_{EX}^{t_{2g}}(x)$.

Generally, due to the inclusion of the effective coulomb interaction term all the composition possess semiconductor energy band-gap and exhibits metallic character if we neglect U_{eff}. In general, in the GGA calculations, the DOS of B-sites Co would lie at the Fermi level, however, incorporation of GGA + U calculation breaks the symmetry of the d-orbitals and distribute the states on both the sides of the Fermi level which creates the valence and conduction band [68]. Additionally, the tetragonal distortion present in the system is quite small. This happens because the local symmetry barely breaks and as a result the localization of d-states is observed in the DOS plots. Thus, the incorporation of suitable U_{eff} would give the precise semiconductor band-gap along with appropriate localization of the states. Therefore, in order to determine the Jahn–teller elongation Δ_{JT} at t_{2g} and e_g states for the octahedral Co we used the relations [67]: (i) $\Delta_{JT}^{e_g\uparrow} = |d^{\uparrow}_{x^2-y^2} - d^{\uparrow}_{z^2}|$, (ii) $\Delta_{JT}^{e_g\downarrow} = |d^{\downarrow}_{x^2-y^2} - d^{\downarrow}_{z^2}|$, (iii) $\Delta_{JT}^{t_{2g}\uparrow} = |d^{\uparrow}_{xy} - d^{\uparrow}_{xz/yz}|$, and (iv) $\Delta_{JT}^{t_{2g}\downarrow} = |d^{\downarrow}_{xy} - d^{\downarrow}_{xz/yz}|$. Figure 7 shows the Δ_{JT} as a function of composition for the octahedral Co ions which is mainly responsible for the tetragonal distortion. From the plot it is quite evident that $\Delta_{JT}^{e_g\downarrow}$ increases with composition and shows a hump across $x = 0.5$ ($\Delta_{JT}^{e_g\downarrow} =$ 0.8 eV) and for $x = 1.0$, $\Delta_{JT}^{e_g\downarrow}$ is maximum with 0.9 eV. The maximum (∼0.4 eV) and minimum (0.1 eV) value of $\Delta_{JT}^{e_g\uparrow}$ occur at $x = 0.0$ and 0.75, respectively. For $x \leqslant 0.125$ case both the parameters $\Delta_{JT}^{t_{2g}\uparrow}$ and $\Delta_{JT}^{t_{2g}\downarrow}$ exhibit negligibly small magnitudes, but for $x = 1.0$ both the quantities gradually increase and reaches 0.5 eV. For AFM $GeCo_2O_4$ the magnitude of Δ_{JT} is significantly high (∼0.9 eV). Such enhanced crystal field splitting controls the energy band gap (E_g) of the system which is the main reason that this pyrochlore system exhibits the maximum E_g than the remaining compositions of the series. Furthermore, the splitting of the d-orbitals significantly influences the interaction between the spins and as a result we obtain high exchange interaction between the B-site Co ions ($J_{BB} \sim -22.3$ meV) for $x = 1.0$.

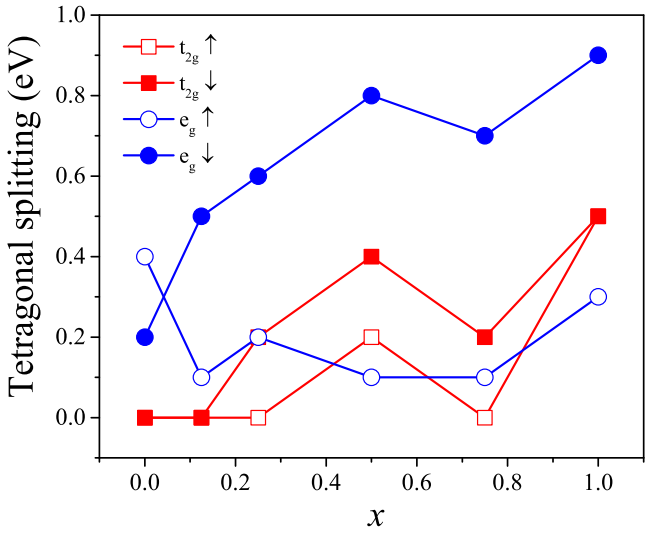

Figure 7. The tetragonal splitting (Δ_{JT}) for different compositions (x) obtained from the DOS calculations for the B-site Co in $Co_2Ti_{1-x}Ge_xO_4$ system.

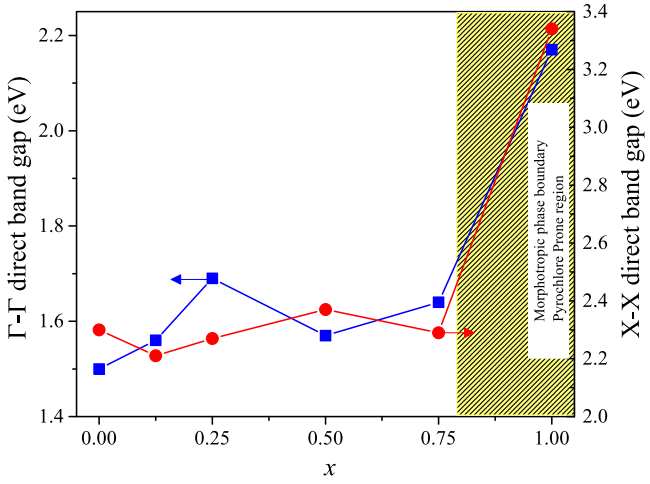

Figure 8. The magnitude of energy direct band gap (E_g) along symmetry directions Γ and X for different compositions of $Co_2Ti_{1-x}Ge_xO_4$. Significant change in direct band gap is noticeable for $x > 0.75$, indicating the change in the structure. The region above $x > 0.75$ is also shown with a yellow shaded domain indicating the morphotropic phase boundary.

In our calculations, we used three distinct magnitudes of $U_{\text{eff}} = 4, 2$ and 0 eV for the cations Co, Ti and Ge atoms, respectively and performed the band structure calculation across different symmetry points in the Brillouin zone by considering the ground state configurations of different compositions as shown in figure 8. Consequently, our calculations reveal the direct energy band-gap values at $\Gamma(X)$ symmetry point: $E_g \sim 1.7$ eV (2.2 eV) and 1.8 eV (3.3 eV) for Co_2TiO_4 ($x = 0$) and $GeCo_2O_4$ ($x = 1$), respectively. These results are in good agreements with previously reported experimental results and theoretical findings based on *ab initio* studies [30]. While incorporating Ge in Co_2TiO_4 matrix, the X-X direct band gap does not show any major change except a small increase across $x = 0.25$ and 0.75 with 1.9 eV and 1.8 eV. In case of Γ-Γ direct band gap, the magnitude of E_g varies between 2.2 eV (for $x = 0$) and 2.3 eV (for $x = 0.875$). Nevertheless, for $x = 1.0$ the X-X direct band gap increases significantly to 3.3 eV. The main origin of such sudden increase in the band gap energy can be clearly understood from the DOS plots. For $x = 1$ ($GeCo_2O_4$ case), the direct band gap occurs due to charge transfer between O($2p$) and Co^{2+} (e_g) states, while, for the remaining compositions Ti-t_{2g} states emerges near the Fermi level in the conduction band and initiate the charge transfer between O($2p$) and Ti^{4+} (t_{2g}) states.

On the other hand, the magnetic properties of the system are quite interesting in the sense that for all the values of x and y overall system exhibits FiM behaviour except for the case of $x = 1.0$ and $y = 1.0$ (i.e., $GeCo_2O_4$) in which the system exhibits a perfect AFM ordering. These features are clearly visible in the DOS calculations. In table 3S we present the magnitude of all the individual and total magnetic moments (μ_B) for various combinations of x and y in $Co_2Ti_{1-x}Ge_xO_4$ lattice [60]. Our calculations suggest that the magnitude of Co moment at A- and B-sites are nearly same in magnitude, but with opposite spin orientations 2.70 μ_B and -2.71 μ_B, respectively. For $y = 0.0$, for different compositions the number of Co atoms in A- and B-sites is constant and as a result the total moment ($\Delta\mu$) remains nearly equal. However, this behaviour is not continued for $y = 0.5$ and 1.0. For $y = 0.5$, $\Delta\mu$ changes from -0.4 μ_B ($x = 0.125$) to -2.96 μ_B ($x = 1.0$) and in the case of $y = 1.0$, the total moment increases from -1.50 μ_B ($x = 0.125$) to -4.43 μ_B ($x = 0.75$). The $\Delta\mu$ gradually increases with x due to the imbalance of Co atoms between the A- and B-sites. On the other hand, for any composition, for $y = 1.0$ the number of Co occupying the B-sites are always higher than for $y = 0.5$ as results the $\Delta\mu$ is always larger for $y = 1.0$ as compared to the other two configurations. Another interesting finding is that for any composition the magnetic moment corresponding to A-site Co reduces with increasing 'y', because of the substitution of non-magnetic Ge^{4+} at the A-site and such dilution causes significant increase of Co^{2+} ions migrating to octahedral sites. This feature is quite significant for all the compositions greater than 0.5.

On the other hand, the experimental studies on this series is first reported way back in 1976 by Strooper *et al* [48]. These authors reported detailed magnetic properties for different compositions up to $x = 0.4$ ($Ti_{0.6}Ge_{0.4}Co_2O_4$) in which they noticed significant reduction in the ordering temperatures (53 K ± 2 to 39 K ± 2 for $x = 0$ to 0.4, respectively) and mean exchange interactions J_{AB} (-6.3 K ± 0.3 to -5.8 K ± 0.3 for $x = 0$ to 0.4, respectively) without any major changes in J_{AA} and J_{BB}. The temperature dependence of magnetization studies reported by these authors show no systematic variation of the sub-lattice magnetization ($M_A(0)$ and $M_B(0)$) and Curie-constant (C) as a function of composition of the system: C ($=N_A\mu^2/3k_B$) for $x = 0$ is $C = 5.4$ cc K mol^{-1} and $M_A(0)$ ($=M_B(0)$) ~20 450 G mol^{-1} cm^{-3} and these quantities remain constant with increasing x up till 0.4 [48]. It is important to note that Strooper *et al* considered that Ge atoms are favourable to occupy the B-sites which in our calculations correspond to the structure for $y = 0$. Accordingly, our calculation results for $y = 0$ yield constant magnetic moment for

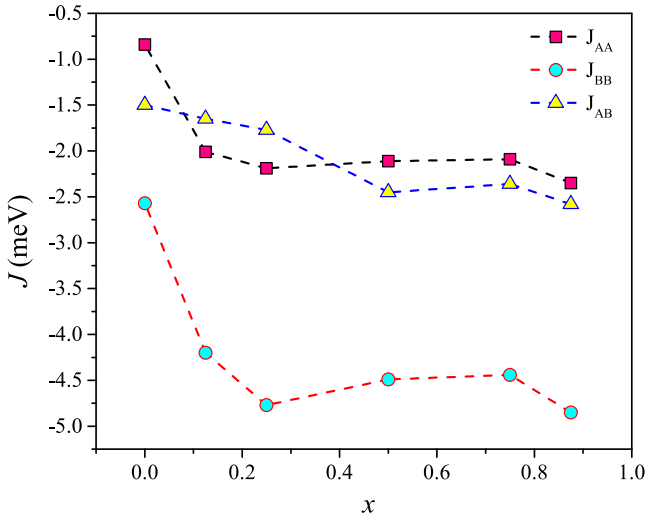

Figure 9. Compositional variation of the magnetic exchange parameters (J_{ij}) for $y = 0$ of $Co_2Ti_{1-x}Ge_xO_4$. J_{BB} dominates over other interactions for $x > 0.25$.

different compositions of x which is consistent with the results of Strooper *et al* [48]. In the present case we evaluated the exchange interaction using the Heisenberg Hamiltonian:

$$H = -\sum_{\langle ij \rangle} J_{ij}\vec{S}_i \cdot \vec{S}_j, \tag{2}$$

where $\langle ij \rangle$ represents the summation over the nearest neighbour sites i and j and S is the corresponding spin of the magnetic ions [58, 59, 65, 69, 70]. In the present case we considered the collinear spin configuration and calculated the total energies of the system for four different spin state configurations. Further this calculated energies were substituted in equation (2) and first nearest neighbour exchange interactions: J_{AA}, J_{BB} and J_{AB} were computed. Figure 9 depicts the variation of J_{AA}, J_{BB} and J_{AB} for different compositions of x ($y = 0$) which are AFM in nature. For $x = 0.0$, $J_{AA} = -0.8$ meV and it increases with increasing the composition up to -2.01 meV till x reaches 0.125, beyond this composition, no significant increase in J_{AA} is noticed (it reaches maximum value -2.4 meV for $x = 0.875$). Almost similar trend has been noticed in case of J_{BB} except very high magnitude ~ -4.9 meV for $x = 0.875$ and comparable to J_{AA}, J_{BB} does not varies much beyond $x = 0.125$. However, $J_{AB}(x)$ shows a different variation altogether with a maximum value of ~ -2.6 meV for $x = 0.875$. These variations in exchange interactions are not in consonance with the variation of bond length as a function of x. As we substitute the Ge atoms in place of Ti atoms, the size mismatch between the ions may tilt and/or rotate the CoO_6 oxygen octahedral as a result small local distortion occurs which in turn play a key role on the exchange interactions. In case of $GeCo_2O_4$, the exchange interaction is significantly high ($J_{BB} = -22.3$ meV) due to its unique pyrochlore AFM structure. Previous experimental studies by Diaz *et al* reported very high magnetic (orbital) frustration in this system due to the competing exchange interactions acting between the TRI and KGM planes [36]. Nevertheless, using the DFT + U techniques we have been able to obtain only the first nearest neighbour interaction and the calculated J_{ij} (at $T = 0$ K) values in the present case are nearly one order higher in magnitude than the previously reported experimental results [43, 48].

4. Conclusions

In conclusion, we have demonstrated that $Co_2Ti_{1-x}Ge_xO_4$ ($0 \leqslant x \leqslant 1$) spinel exhibits disorder driven weak tunable tetragonal distortion due to the alteration in the energy levels of non-degenerate d_{z^2} and $d_{x^2-y^2}$ orbitals of B-site Co. We find that for $c/a < 1$, the alternation takes place for $E(d_{z^2}) > E(d_{x^2-y^2})$ while for $c/a > 1$, that happens for $E(d_{z^2}) < E(d_{x^2-y^2})$. In addition we also obtain a large exchange splitting $\Delta^{t_{2g}}_{EX-Tet}$ ($\Delta^{e_g}_{EX-Oct}$) for Co^{2+} than those present in the crystal field splitting (Δ_{CF}). Ge atoms prefer to occupy at the octahedral B-site for lower and intermediate substitution levels and forms energetically favourable ground state. However, on approaching the morphotropic phase boundary ($x > 0.75$), Ge atoms start occupying the tetrahedral A-site. The Jahn–Teller distortion, Δ_{JT} in these solid-solutions are linked with the large e_g majority spin splitting (Δ_{JT-e_g}) driven by the enhanced crystal field splitting which essentially controls the energy band-gap (1.7 eV ($E_{g-\Gamma\Gamma}$) $\leqslant E_g \leqslant$ 3.3 eV (E_{g-XX})) of the investigated system for all the combinations of x and y. For $x = y = 1$, the $E_{g-XX} \sim 3.3$ eV is associated with the inter-band charge transfer transition, $O(2p) \rightarrow Co^{2+}(e_g)$. However, for the remaining compositions, Ti-t_{2g} states emerge near the Fermi-level (E_F) in the conduction band and thus the E_g departs from 1.7 eV as the charge transfer takes place between $O(2p)$ and Ti^{4+} (t_{2g}) states. The magnetic structure is mainly determined by the high spin configuration of Co^{2+} ions, and for any combinations of x and y the system is FiM in nature, except for $x = 1.0$ and $y = 1.0$ the system ($GeCo_2O_4$) possesses perfect AFM ordering. Under no disorder case ($y = 0$), the net magnetic moment ($\Delta\mu$) remains constant, whereas for non-zero values of y the magnitude of $\Delta\mu$ increases with x due to the imbalance of number density of Co atoms between the A- and B-sites. The AFM exchange interaction J_{BB} dominates over J_{AA} and J_{AB} for all the compositions except for $x = y = 1.0$. Nonetheless, for $x > 0.125$, the strength of J_{AA} and J_{BB} does not change significantly whereas J_{AB} gradually increases with x.

Data availability statement

All data that support the findings of this study are included within the article (and any supplementary files).

Acknowledgments

SG acknowledge Fund for Improvement of Science and Technology (FIST) programme of Department of Science and Technology, India, for partial support of this work (Grant No. SR/FST/PSII-037/2016). SG also thank the Central Instruments Facility (CIF)-IIT Guwahati for partial support of this

work. The authors would like to thank IIT Guwahati and DST India for the PARAM Supercomputing facility and the computer cluster in the Department of Physics, IIT Guwahati (Grant No. SR/FST/PII/020/2009), respectively.

ORCID iDs

Subhash Thota https://orcid.org/0000-0003-0740-2195

References

[1] Sakamoto N 1962 Magnetic properties of cobalt titanate *J. Phys. Soc. Japan* **17** 99–102

[2] Hubsch J and Gavoille G 1982 Semi-spin-glass behavior in the Co_2TiO_4 compound *Phys. Rev.* B **26** 3815

[3] Gavoille G, Hubsch J and Koutani S 1991 Random anisotropy in the Co_2TiO_4 compound *J. Magn. Magn. Mater.* **102** 283–6

[4] Srivastava J K, Kulkarni J A, Ramakrishnan S, Singh S, Marathe V R, Chandra G, Darshane V S and Vijayaraghavan R 1987 The spin glass behaviour of disordered spinel ferrite Co_2TiO_4 *J. Phys. C: Solid State Phys.* **20** 2139

[5] Nayak S *et al* 2015 Magnetic compensation, field-dependent magnetization reversal, and complex magnetic ordering in Co_2TiO_4 *Phys. Rev.* B **92** 214434

[6] Thota S *et al* 2017 Neutron diffraction study of the inverse spinels Co_2TiO_4 and Co_2SnO_4 *Phys. Rev.* B **96** 144104

[7] Nagata T 1961 *Rock Magnetism* 2nd edn (Tokyo: Maruzen)

[8] Néel M L 1948 Propriétés magnétiques des ferrites; ferrimagnétisme et antiferromagnétisme *Ann. Phys.* **12** 137–98

[9] Kumar A and Yusuf S M 2015 The phenomenon of negative magnetization and its implications *Phys. Rep.* **556** 1–34

[10] Manna P K, Yusuf S M, Shukla R and Tyagi A K 2010 Coexistence of sign reversal of both magnetization and exchange bias field in the core–shell type $La_{0.2}Ce_{0.8}CrO_3$ nanoparticles *Appl. Phys. Lett.* **96** 242508

[11] Shukla R, Bera A K, Yusuf S M, Deshpande S K, Tyagi A K, Hermes W, Eul M and Pöttgen R 2009 Multifunctional nanocrystalline $CeCrO_3$: antiferromagnetic, relaxor, and optical properties *J. Phys. Chem.* C **113** 12663–8

[12] Shukla R, Manjanna J, Bera A K, Yusuf S M and Tyagi A K 2009 $La_{1-x}Ce_xCrO_3$ ($0.0 \leqslant x \leqslant 1.0$): a new series of solid solutions with tunable magnetic and optical properties *Inorg. Chem.* **48** 11691–6

[13] Adachi H and Ino H 1999 A ferromagnet having no net magnetic moment *Nature* **401** 148–50

[14] Chen X, Wang K, Hor P, Xue Y and Chu C 2005 Anomalies at the compensation temperature in the zero-magnetization ferromagnet (Sm, Gd)Al_2 *Phys. Rev.* B **72** 054436

[15] Adachi H, Kawata H, Hashimoto H, Sato Y, Matsumoto I and Tanaka Y 2001 Zero-magnetization ferromagnet proven by helicity-switching Compton scattering *Phys. Rev. Lett.* **87** 127202

[16] Taylor J, Duffy J, Bebb A, Lees M, Bouchenoire L, Brown S and Cooper M 2002 Temperature dependence of the spin and orbital magnetization density in $Sm_{0.982}Gd_{0.018}Al_2$ around the spin–orbital compensation point *Phys. Rev.* B **66** 161319

[17] Prejbeanu I L, Kerekes M, Sousa R C, Sibuet H, Redon O, Dieny B and Nozières J P 2007 Thermally assisted MRAM *J. Phys.: Condens. Matter.* **19** 165218

[18] Pebley A C, Fuks P E, Pollock T M and Gordon M J 2016 Exchange bias and spin glass behavior in biphasic $NiFe_2O_4$/NiO thin films *J. Magn. Magn. Mater.* **419** 29–36

[19] Nogués J *et al* 2005 Exchange bias in ferromagnetic nanoparticles embedded in an antiferromagnetic matrix *Int. J. Nanotechnol.* **2** 23–42

[20] Artus M, Ammar S, Sicard L, Piquemal J-Y, Herbst F, Vaulay M-J, Fiévet F and Richard V 2008 Synthesis and magnetic properties of ferrimagnetic $CoFe_2O_4$ nanoparticles embedded in an antiferromagnetic NiO matrix *Chem. Mater.* **20** 4861–72

[21] Tian Z M, Yuan S L, Yin S Y, Liu L, He J H, Duan H N, Li P and Wang C H 2008 Exchange bias effect in a granular system of $NiFe_2O_4$ nanoparticles embedded in an antiferromagnetic NiO matrix *Appl. Phys. Lett.* **93** 222505

[22] Del Bianco L, Fiorani D, Testa A M, Bonetti E and Signorini L 2004 Field-cooling dependence of exchange bias in a granular system of Fe nanoparticles embedded in an Fe oxide matrix *Phys. Rev.* B **70** 052401

[23] Giri S, Patra M and Majumdar S 2011 Exchange bias effect in alloys and compounds *J. Phys.: Condens. Matter.* **23** 073201

[24] Ghosh S, Joshi D C, Pramanik P, Jena S K, Pittala S, Sarkar T, Seehra M S and Thota S 2020 Antiferromagnetism, spin-glass state, H–T phase diagram, and inverse magnetocaloric effect in Co_2RuO_4 *J. Phys.: Condens. Matter.* **32** 485806

[25] Nayak S *et al* 2016 Low-temperature anomalous magnetic behavior of Co_2TiO_4 and Co_2SnO_4 *J. Appl. Phys.* **120** 163905

[26] Nayak S, Joshi D C, Krautz M, Waske A, Eckert J and Thota S 2016 Reentrant spin-glass behavior and bipolar exchange-bias effect in 'Sn' substituted cobalt-orthotitanate *J. Appl. Phys.* **119** 043901

[27] Pramanik P, Joshi D C, Reehuis M, Hoser A, Hoffmann J-U, Manna R S, Sarkar T and Thota S 2020 Neutron diffraction evidence for local spin canting, weak Jahn–Teller distortion, and magnetic compensation in Ti_{1-x} $Mn_xCo_2O_4$ spinel *J. Phys.: Condens. Matter.* **32** 245801

[28] Thota S and Seehra M S 2013 Co-existence of ferrimagnetism and spin-glass state in the spinel Co_2SnO_4 *J. Appl. Phys.* **113** 203905

[29] Thota S, Narang V, Nayak S, Sambasivam S, Choi B C, Sarkar T, Andersson M S, Mathieu R and Seehra M S 2015 On the nature of magnetic state in the spinel Co_2SnO_4 *J. Phys.: Condens. Matter.* **27** 166001

[30] Ghosh S, Singh S, Joshi D C, Pramanik P, Ghosh S, Mishra P K and Thota S 2018 Role of dilution on the electronic structure and magnetic ordering of spinel cobaltites *Phys. Rev.* B **98** 235119

[31] Prosnikov M A, Molchanova A D, Dubrovin R M, Boldyrev K N, Smirnov A N, Davydov V Y, Balbashov A M, Popova M N and Pisarev R V 2016 Lattice dynamics and electronic structure of cobalt–titanium spinel Co_2TiO_4 *Phys. Solid State* **58** 2516–22

[32] Fu Q S, Li C L, Meng B, Chakrabarti C, Zhang R, Chen X H, Li Y H and Yuan S L 2019 Effect of annealing temperature on structural and magnetic properties of Co_2TiO_4 ceramics prepared by sol-gel method *Ceram. Int.* **45** 6906–11

[33] Anderson P W 1956 Ordering and antiferromagnetism in ferrites *Phys. Rev.* **102** 1008

[34] Hubsch J and Gavoille G 1987 First order magnetic phase transition in $GeCo_2O_4$ *J. Magn. Magn. Mater.* **66** 17–22

[35] Matsuda M, Hoshi T, Aruga Katori H, Kosaka M and Takagi H 2011 Magnetic-field-induced transitions in spinel $GeCo_2O_4$ *J. Phys. Soc. Japan* **80** 034708

[36] Diaz S, De Brion S, Chouteau G, Canals B, Simonet V and Strobel P 2006 Magnetic frustration in the spinel compounds $GeCo_2O_4$ and $GeNi_2O_4$ *Phys. Rev.* B **74** 092404

[37] Fabrèges X *et al* 2017 Field-driven magnetostructural transitions in $GeCo_2O_4$ *Phys. Rev.* B **95** 014428

[38] Watanabe T, Hara S and Ikeda S-I 2008 Jahn–Teller inactivity and magnetic frustration in $GeCo_2O_4$ probed by ultrasound velocity measurements *Phys. Rev.* B **78** 094420

[39] Sim G and Lee S 2018 Discovery of a new type of magnetic order on pyrochlore spinels *Phys. Rev.* B **98** 014423

[40] Hoshi T, Aruga Katori H, Kosaka M and Takagi H 2007 Magnetic properties of single crystal of cobalt spinel $GeCo_2O_4$ *J. Magn. Magn. Mater.* **310** e448–50

[41] Lashley J, Stevens R, Crawford M, Boerio-Goates J, Woodfield B, Qiu Y, Lynn J, Goddard P and Fisher R 2008 Specific heat and magnetic susceptibility of the spinels $GeNi_2O_4$ and $GeCo_2O_4$ *Phys. Rev.* B **78** 104406

[42] Barton P T, Kemei M C, Gaultois M W, Moffitt S L, Darago L E, Seshadri R, Suchomel M R and Melot B C 2014 Structural distortion below the Néel temperature in spinel $GeCo_2O_4$ *Phys. Rev.* B **90** 064105

[43] Pramanik P, Ghosh S, Yanda P, Joshi D, Pittala S, Sundaresan A, Mishra P, Thota S and Seehra M 2019 Magnetic ground state, field-induced transitions, electronic structure, and optical band gap of the frustrated antiferromagnet $GeCo_2O_4$ *Phys. Rev.* B **99** 134422

[44] Jin S, Yang G, Song H, Cui H and Wang C 2015 Ultrathin hexagonal 2D Co_2GeO_4 nanosheets: excellent Li-storage performance and ex situ investigation of electrochemical mechanism *ACS Appl. Mater. Interfaces* **7** 24932–43

[45] Yuvaraj S, Park M-S, Kumar V G, Lee Y S and Kim D-W 2017 Electrochemical performance of M_2GeO_4 (M = Co, Fe and Ni) as anode materials with high capacity for lithium-ion batteries *J. Electrochem. Sci. Technol.* **8** 323–30

[46] Romeijn F C 1953 *Physical and Crystallographical Properties of Some Spinels* (Leiden: Rijksuniversiteit)

[47] Reinen D 1968 Ligandenfeldeffekte und Struktur oxidischer Feststoffe. II Ge^{4+} und Si^{4+} haltige Olivinphasen *Z. Anorg. Allg. Chem.* **356** 182–8

[48] De Strooper K, Govaert A, Dauwe C and Robbrecht G 1976 Magnetic properties of the spinel series $Co_2Ge_xTi_{1-x}O_4$ ($0 \leqslant x \leqslant 1$) *Phys. Status Solidi* A **37** 127–32

[49] Hohenberg P and Kohn W 1964 Inhomogeneous electron gas *Phys. Rev.* **136** B864

[50] Kohn W and Sham L J 1965 Self-consistent equations including exchange and correlation effects *Phys. Rev.* **140** A1133

[51] Kresse G and Furthmüller J 1996 Efficient iterative schemes for *ab initio* total-energy calculations using a plane-wave basis set *Phys. Rev.* B **54** 11169

[52] Kresse G and Furthmüller J 1996 Efficiency of *ab-initio* total energy calculations for metals and semiconductors using a plane-wave basis set *Comput. Mater. Sci.* **6** 15–50

[53] Kresse G and Hafner J 1993 *Ab initio* molecular dynamics for liquid metals *Phys. Rev.* B **47** 558

[54] Perdew J P, Burke K and Ernzerhof M 1996 Generalized gradient approximation made simple *Phys. Rev. Lett.* **77** 3865

[55] Dudarev S L, Botton G A, Savrasov S Y, Humphreys C J and Sutton A P 1998 Electron-energy-loss spectra and the structural stability of nickel oxide: an LSDA + U study *Phys. Rev.* B **57** 1505–9

[56] Zunger A, Wei S-H, Ferreira L G and Bernard J E 1990 Special quasirandom structures *Phys. Rev. Lett.* **65** 353

[57] Vanpoucke D E, Bultinck P, Cottenier S, Van Speybroeck V and Van Driessche I 2011 Density functional theory study of $La_2Ce_2O_7$: disordered fluorite versus pyrochlore structure *Phys. Rev.* B **84** 054110

[58] Das D and Ghosh S 2016 First-principles investigations into the thermodynamics of cation disorder and its impact on electronic structure and magnetic properties of spinel $Co(Cr_{1-x}Mn_x)_2O_4$ *J. Phys.: Condens. Matter.* **29** 055805

[59] Das D, Ganguly S, Sanyal B and Ghosh S 2016 Effect of Fe doping in the structural, electronic and magnetic properties of $CoCr_2O_4$: insights from *ab initio* calculations *Mater. Res. Express* **3** 106106

[60] See the supplemental material for the additional information crystal structure parameters (bond-lengths and lattice constants), density of states and magnetic moments of $Co_2Ti_{1-x}Ge_xO_4$ for different combinations of x and y.

[61] Diaz S, de Brion S, Holzapfel M, Chouteau G and Strobel P 2004 Study of competitive magnetic interactions in the spinel compounds $GeNi_2O_4$, $GeCo_2O_4$ *Physica* B **346–347** 146–9

[62] Navrotsky A and Kleppa O J 1967 The thermodynamics of cation distributions in simple spinels *J. Inorg. Nucl. Chem.* **29** 2701–14

[63] Kriessman C J and Harrison S E 1956 Cation distributions in ferrospinels. Magnesium–manganese ferrites *Phys. Rev.* **103** 857

[64] Dunitz J D and Orgel L E 1957 Electronic properties of transition-metal oxides—I: distortions from cubic symmetry *J. Phys. Chem. Solids* **3** 20–9

[65] Das D and Ghosh S 2015 Density functional theory based comparative study of electronic structures and magnetic properties of spinel ACr_2O_4 (A = Mn, Fe, Co, Ni) compounds *J. Phys. D: Appl. Phys.* **48** 425001

[66] Ghosh S, Jena S K, Mishra P K, Seehra M S and Thota S 2019 Magnetic exchange interactions and band gap bowing in $Ni_xMg_{1-x}O$ ($0.0 \leqslant x \leqslant 1.0$): a GGA + U density functional study *J. Appl. Phys.* **126** 233904

[67] Wulandari R D, Muhammady S and Darma Y 2020 Tuning spin state of Ru^{4+} ion and Jahn–Teller distortion in cubic $SrRuO_3$ system by controlling in-plane strain: a first-principle study *J. Phys. Chem. Solids* **137** 109225

[68] Kittel C, McEuen P and McEuen P 1996 *Introduction to Solid State Physics* vol 8 (New York: Wiley)

[69] Xiang H, Kan E, Wei S-H, Whangbo M-H and Gong X 2011 Predicting the spin-lattice order of frustrated systems from first principles *Phys. Rev.* B **84** 224429

[70] Zhu X, Edström A and Ederer C 2020 Magnetic exchange interactions in $SrMnO_3$ *Phys. Rev.* B **101** 064401